Electronic behaviour of Au-Pt alloys and the 4f binding energy shift anomaly in Au bimetallics- X-ray spectroscopy studies

Cite as: AIP Advances **8**, 065210 (2018); https://doi.org/10.1063/1.5027251
Submitted: 28 February 2018 • Accepted: 30 May 2018 • Published Online: 12 June 2018

Dongniu Wang, Xiaoyu Cui, Qunfeng Xiao, et al.

AIP ADVANCES **8**, 065210 (2018)

Electronic behaviour of Au-Pt alloys and the 4f binding energy shift anomaly in Au bimetallics- X-ray spectroscopy studies

Dongniu Wang,[1,2] Xiaoyu Cui,[2] Qunfeng Xiao,[2] Yongfeng Hu,[2] Zhiqiang Wang,[1] Y. M. Yiu,[1] and T. K. Sham[1,a]

[1]*Department of Chemistry and Soochow - Western Centre for Synchrotron Radiation Research, University of Western Ontario, London, Ontario, Canada, N6A 5B7*

[2]*Canadian Light Source, Saskatoon, Saskatchewan, Canada, S7N 2V3*

(Received 28 February 2018; accepted 30 May 2018; published online 12 June 2018)

The electronic structure and charge redistribution of 6s conduction charge and 5d charge in Au and Pt alloys, Au_9Pt and $AuPt_9$ have been investigated using a charge compensation model. It is found that, both the Au and Pt 4f binding energy (BE) exhibits a negative shift in the alloys relatively to the pure metal in apparent disagreement with electroneutrality considerations (Au is the most electronegative metallic element); more interestingly, the negative Au 4f BE shift in Au-Pt alloy is in contrast to previous observations for a large number of Au bimetallic systems with more electropositive hosts in which the more electropositive the host,, the more positive the Au 4f BE shift. This anomaly is counter intuitive to electronegativity considerations. This dilemma was resolved by the charge compensation model in which both electronegativity and charge neutrality can be satisfied and the overall charge flow δ, onto Au is small and positive and δ arises from charge flow of 6s conduction charge, Δn_c onto Au site, which is partially compensated by the depletion of 6d charge Δn_d at the Au site ($\delta = \Delta n_c + \Delta n_d \sim 0.1 > 0$). The much larger Coulomb interaction between 4f and 5d than that between 4f and 6s results in positive 4f BE shifts. The Au 4f BE shift in Au-Pt alloys together with ^{193}Au Mössbauer data were used in the charge compensation model analysis which shows that the model is still valid in that the Au 4f shift in Au-Pt alloy arises from mainly conduction charge gain with little depletion of d charge at the Au site. The model also works for Pt. The Au and Pt 5d character in the alloys have been examined with valence band spectra which show both maintain their d characteristic in dilute alloys with Pt d piling up at the Fermi level, and the top of the Au valence band being pushed toward the Fermi level; this is confirmed with DFT densities of state calculations. When Pt is diluted in Au, it gains d charge as evident from the reduction in whiteline intensity at the Pt L_3-edge XANES. What emerges from this work is a picture in which the s-d charge compensation in Au bimetallic alloys is triggered by electronegativity difference between Au and the host. For Au-Pt and Au-Pd systems, the difference in electronegativity is very small, conduction charge transfer dominates, and the Au 4f shift is negative whereas in most Au bimetallics, the larger the electronegativity difference, the larger the compensation and the larger the Au 4f shifts. https://doi.org/10.1063/1.5027251

I. INTRODUCTION

The electronic structure of bimetallic Au systems exhibits some peculiar behaviour leading to an apparent anomaly in the Au 4f binding energy shifts[1–4]- that is that in Au-metalloid intermetallic

[a]Corresponding author: tsham@uwo.ca

systems, including compounds and random alloys, such as $AuAl_2$, $AgGa_2$, $AuTe_2$[5] and AuZn[6] etc. as well as Au-3d, 4d and 5d metal alloys and compounds, such as Au diluted in 3d transition metals and a series of Au-Cu[7,8] and Au-Ag[9] alloys, as well as Au-Ti[10] and Au-Ta[11] metallic compounds, the Au 4f binding energy shift in alloys relative to that of Au metal is always positive, indicating charge depletion at the Au site upon alloying. In fact, the larger the electronegativity difference between the host and Au, the lager the positive Au 4f shift. This is in contrast to the electronegativity expectation that Au, the most electronegative element among all metallic elements, should attract electron charge hence a negative shift is expected. The electronegativity according to Pauling's scale is 2.4 for Au, 2.2 for Pd and Pt, 1.5 for Al; yet $AuAl_2$ intermetallic exhibits the largest 4f shift of 1.95 eV[12]! This positive binding energy shift is also in apparent disagreement with ^{197}Au Mössbauer isomer shift (IS)[1,13–17] which measures the contact density at the nucleus and is in line with electronegative arguments, i.e., that, the larger the electronegativity difference between Au and the other metallic component in the bimetallic system, the larger the IS (larger contact density). $AuAl_2$ has the largest IS of 7.6 mms^{-1}[13]! On the other hand, it is expected that in metallic system, electroneutrality holds, that is that the net charge flow on and off a site should be nearly zero.

This apparent dilemma was finally resolved by the introduction of a charge compensation model by Watson et al.[1] which takes into account of the compensation of 6s-like conduction electron gain and 5d charge depletion, together with the appropriate evaluation of the Coulomb integral using a normalized atom method (Wigner-Seitz cell). It was then confirmed that there is little net charge flow indeed between Au and host-metal atoms upon alloying, i.e., that the increase of predominantly s-like conduction-electron count, Δn_c, at the Au site within the Wigner-Seitz volume (expected from electronegativity arguments and evident from Mossbauer IS) is largely but not totally compensated by a depletion in 5d electron count, Δn_d. Since the core level binding energy change by placing an additional 5d electron at the Au site F_d in the renormalized atom acheme[1] is significantly larger than that of an additional 6s conduction electron, F_c, an imbalance 5d charge depletion ($|\Delta n_c| > |\Delta n_d|$) can still lead to a positive 4f binding energy shift. It was found from several analyses that the net charge flow at the Au site, $\delta = \Delta n_c + \Delta n_d$, is positive but very small ($\sim$ 0.1 electron) and that the ratio $\Delta n_c/\Delta n_d$ is surprisingly constant given the various numerical uncertainties of the analysis.[2–4] It thus appears that the Au d bands are actively involved through hybridization in alloying, and that such s-d compensation is a general characteristic of Au alloys. Substantial hybridization of the Au d bands with the Au non-d states and with the valence states of host metal atoms is observed in the valence-band spectra. The relationship of this hybridization to the d and non-d charge-transfer effects inferred from the core level and Mössbauer shifts was later confirmed with X-ray Absorption Near Edge Structure (XANES) measurements of the whiteline (WL) intensity at the Au $L_{3,2}$-edge, which tracks the unoccupied states of 5d character, primarily $5d_{5/2}$ in Au and Pt.[9,16,17]

Despite considerable work on the electronic behavior of Au bimetallic systems, experimental studies of Au-Pt alloys are relatively lacking albeit there have been further theoretical investigations on the effect of electron redistribution in bimetallic systems on surface and bulk binding energy shifts.[18,19] Au and Pt are interesting 5d noble metals in that, the relativistic effect of the 5 d electrons are large; this leads to the dominance of the $5d_{5/2}$ and $5d_{3/2}$ character. Au and Pt are the most and second most electronegative metallic elements according to Pauling's electronegativity scale. In the case of Au metal (nominal electronic configuration in the solid: $6s^15d^{10}$), the d band is full, the top of the d band is $\sim$ 2 eV below the Fermi level where the Fermi edge is essentially 6s conduction character; the combined effect of spin-orbit coupling (atomic value is $\sim$ 1 eV) and d band formation results in a broad d band with an apparent spin-orbit splitting of ~2.6 eV (separation of the d band doublet) with the d band centroid at $\sim$ 4.6 eV below the Fermi level. In the case of Pt metal ($6s^15d^9$) however, the d band is not completely filled, the 5d-6s hybridization is more extensive leading to a wider d band than Au; the top of the occupied d band is at the Fermi level and it exhibits narrow unoccupied densities of states (DOS) of $5d_{5/2}$ character just above the Fermi level as evident from the $L_{3,2}$-edge WL intensity anomaly.[20–23] The presence of unoccupied d states above the Fermi level also leads to the asymmetric shape of the Pt 4f peaks, due to many-body effects, known as the Doniac-Sunjic (DS) asymmetry as compared to the more symmetric Au 4f.[24,25] It is this unoccupied d states that lead to

the catalytic properties of Pt.[26–30] One may then ask what the electronic structure is in terms of s-d hybridization in Au-Pt alloys and how it is manifested in the 4f binding energy shift, Mossbauer IS and the occupied and unoccupied d states across the Fermi level in valence band (VB) and $L_{3,2}$-edge XANES and WL intensity measurements.

The advent of nanotechnology has led to the synthesis of Au-Pt nano systems such as nanoparticles and nanowires which exhibit controllable catalytic behavior.[26–30] Interestingly, it was reported that in Au-Pt bimetallic particles, both the Au and Pt 4f binding energy exhibit a negative shift relative to that of the pure metal, an anomaly among the anomaly of Au 4f binding energy shift in Au bimetallics.[4] Also, ^{119}Au Mössbauer of Au-Pt nanoparticles exhibit a small but measurable positive IS.[30] At first glance, these results show that both Au and Pt gain charge upon alloying; this is not in good accord with electronegativity and electroneutrality considerations. Unfortunately, nanostructure results are complicated by its size and morphology dependent behavior, which often lead to different degree of surface segregation, hence chemical inhomogeneity, e.g. forming core-shell structures.[29,30] Thus, we study the above-mentioned issues using bulk alloys in this work. More interesting still, it has also been reported that in Au-Pd alloys, Au 4f also shows a negative shift[31] but the Pd 3d shifts positively. The ^{119}Au Mössbauer shows a positive IS.[32] This seems to be the only case all the binding energy shifts can be straightforwardly interpreted with electronegativity considerations in bimetallic Au alloys. Thus, we will address in this paper not only the specific case of Au-Pt alloy where both Pt and Au 4f shift to lower binding relative to the pure metal but also all Au bimetallic binding energy-electronegativity cases, counter intuitive or in line with electronegativity considerations under the same roof. Bimetallic Au and other noble metal nanostructures and catalysts have become a very trendy topic in contemporary research and technology, in fuel cells for example, where the width and occupancy of the metal d band in the electro-catalyst correlate with catalytic performance;[26] thus, this paper provides the practitioners (often material scientists, chemists and engineers) in these fields a fundamental basis for the interpretation of their data.

In this work, we explore the electronic behavior of Au-Pt bulk alloys by investigating two bulk compositions in the dilute regime, $AuPt_9$ and Au_9Pt. X-ray Photoemission Spectroscopy (XPS) and XANES were used, respectively, to track the 4f binding energy and the VB, and the $L_{3,2}$-edge WL intensity which tracks the unoccupied DOS of $d_{5/2,3/2}$ character above the Fermi level. The experimental results recorded from this work together with ^{119}Au Mössbauer IS from the literature[12–15] are used to analyze the charge redistribution in Au-Pt and Au-Pd[32] systems on the basis of the charge compensation model.[1] The rest of the paper is arranged as follows: Section II describes the experimental procedures and calculations performed to assist the interpretation followed by results in section III then analysis and discussion in section IV and conclusion in section V.

II. EXPERIMENTAL PROCEDURES AND CALCULATIONS

Stoichiometric amount of Au and Pt (10% atomic dilution) were arc melt repeatedly to ensure homogeneity followed by annealing. Au and Pt form random alloys according to the phase diagram.[33] The ingots thus obtained were polished. X-ray diffraction shows that the alloy specimens exhibit patterns characteristic of a fcc crystal structure; there exhibits some broadening and asymmetry indicating a random alloy. XPS measurements were conducted at the Kratos XPS spectrometer of Surface Science Western using monochromatic Al Kα (1486.6 eV), the XPS end-station of the VLS PGM (10-125 eV) beamline[34] using 180 eV photon and the SXRMB (1.7 -10 keV) High Energy XPS (HEXPS) endstation[35] using 2500 eV photon at the Canadian Light Source. Both end-stations at the CLS were equipped with Scienta analyzers operating at 50 eV pass energy. It should be noted that accurate measurements of XPS binding energies (e.g. ±0.01) at the synchrotron requires careful energy calibration and a laboratory source helps ensure the correct calibration. Fortunately, the observed shifts are significant in this analysis and they were carefully calibrated against possible beamline stability due to ring current decay, optics warm-up etc. In XPS measurements, the surface of the specimens was cleaned sequentially in acetone and hexane solutions in an ultrasound bath prior to introduction to the experimental chamber followed by Ar^+ sputtering. It should be noted that in the HEXPS measurement where bulk photoelectrons have sufficient kinetic energy to be detected by the detector, Ar^+ ion sputtering is not always necessary to obtain bulk binding energy shifts.

Au and Pt $L_{3,2}$-edge XANES were collected at the BM beamline of the PNC-XSD, sector 20, at the Advanced Photon Source, Argonne National Laboratory with the storage ring running in a top-up mode. Measurements were made in transmission using multiple layers of fine alloy powders (filed off from the ingots) on Kapton tapes; a Pt or Au foil was used in a three-ion-chamber arrangement to simultaneously calibrate the energy of the X-rays at the Pt and Au L_3-edge.

To assist the interpretation of the VB spectra and the XANES data, we have conducted band structure calculation of the DOS of $Au_{11}Pt$ (more suitable, symmetry wise than Au_9Pt) and $AuPt_{11}$ using the Density Functional Theory (DFT) based WIENk2 code[36–39] and a super cell with the following parameters:

$Au_{11}Pt$ super cell lattice constants

a = b = 4.08 bohr = 2.159 Å, c = 12.24 bohr = 6.4771Å; $\alpha = \beta = \gamma = 90^0$

Atomic sites:

Au (1) at (0, 0, 0); Pt (1) at (0, 0, 0.333333); Au (2) at (0, 0, 0.666667);
Au (3) at (0.5, 0.5, 0); Au (4) at (0.5, 0.5, 0.333333); Au (5) at (0.5, 0.5, 0.666667);
Au (6) at (0.5, 0, 0.1666667); Au (7) at (0.5, 0, 0.5); Au (8) at (0.5, 0, 0.833333);
Au (9) at (0, 0.5, 0.166667); Au (10) at (0, 0.5, 0.5); Au (11) at (0, 0.5, 0.833333)

$AuPt_{11}$ super cell lattice constants

a = b = 3.92 bohr = 2.0744 Å, c = 11.76 bohr = 6.2231Å; $\alpha = \beta = \gamma = 90^0$

Atomic sites:

Pt (1) at (0, 0, 0); Au (1) at (0, 0, 0.333333); Pt (2) at (0, 0, 0.666667); Pt (3) at (0.5, 0.5, 0)
Pt (4) at (0.5, 0.5, 0.333333); Pt (5) at (0.5, 0.5, 0.666667); Pt (6) at (0.5, 0, 0.1666667)
Pt (7) at (0.5, 0, 0.5); Pt (8) at (0.5, 0, 0.833333); Pt (9) at (0, 0.5, 0.166667)
Pt (10) at (0, 0.5, 0.5); Pt (11) at (0, 0.5, 0.833333)

The partial and total DOS averaged over all relevant atoms involved will be presented in the discussion section.

Similar cell parameters have also been used to calculate the Au and Pt 4f bonding energy shifts. The binding energies of Au and Pt in fcc Au, $Au_{11}Pt$, $AuPt_{11}$, and fcc Pt are calculated based on the ground state energies using DFT (Density Functional Theory) with GGA (Generalized Gradient Approximation) and PBE exchange correlation potential[40] and SCF (Self-consistent) calculation with the program, WIEN2k. The calculations are carried out with and without a core hole.

The calculation shows that the calculated binding energies are generally under-estimated by 5-7 eV compared to experiment but the trend is in good agreement; for example, with one core

TABLE I. Relevant parameters[a] for analysis; the bold letter values represent the shift of the diluted components.

Sample	*hv (eV)*	^{197} Au Mössbauer Isomer shift (mm/s)	ΔBE (Au 4f)[b], Alloy – Au (eV)	ΔBE (Pt 4f)[b], Alloy – Pt (eV)
$PtAu_9$	180		- 0.11	**- 0.43**
Pt_9Au	180		**- 0.14**	- 0.05
$PtAu_9$	1486.6	0.08[c]	- 0.11	**- 0.50**
Pt_9Au	1486.6	0.78[c]	**- 0.24**	- 0.09
$PtAu_9$	2500		- 0.04	**- 0.45**
Pt_9Au	2500		**- 0.26**	- 0.09
Pt_4Au (NP)[d]	1486.6		- 0.36	- 0.10
$PtAu_4$ (NP)[d]	1486.6		- 0.10	- 0.59
PtAu quenched[e]		0.41		

[a]This work except noted.

[b]value represents the average of various sites in a random alloy; the linewidth is nearly the same for the Au 4f under similar experimental conditions and the Pt 4f peak becomes a little narrower and less asymmetric in dilute alloys due to charge transfer into the Pt d band which affects the DS parameter in the peak shape.

[c]extrapolated from ref. 30.

[d]ref. 29.

[e]ref 30.

hole the calculated Au 4f ΔBE between $AuPt_{11}$, and Au is -0.52 eV and the Pt 4f ΔBE between $AuPt_{11}$ and Pt is -0.61 eV, in qualitative agreement with experimental values (Table I, block values). Without the core hole, the agreement is also satisfactory, the calculated 4f ΔBE value is in better agreement (-0.25 eV) with experiment for $AuPt_{11}$ and less satisfactory (-0.88 eV) for $PtAu_{11}$. The discrepancy may arise from a slightly compressed and expanded unit cells in $AuPt_{11}$ and $PtAu_{11}$, respectively.

III. RESULTS

Figure 1 shows the Au and Pt 4f region of the alloys and the pure metals recorded using monochromatic Al Kα X-rays. The slight variation of ΔBE using different photon energies is due to slight chemical inhomogeneity of a random alloy, different cross-section[41] and penetration depths of the X-rays[42] and escape depths of the electrons as well as surface contribution,[43] and it does not affect the direction of the shift and the conclusion of the analysis. It is apparent from Figure 1 that (i) in both alloys, the Au 4f and Pt 4f doublet shift to lower binding energy relative to the pure metal; (ii) the shift is noticeably larger for Pt when it is diluted in Au than Au diluted in Pt and the shift increases with dilution; (iii) the peak height ratio is close to the stoichiometric ratio with the majority component slightly depleted. Since the 4f partial photoionization cross-section for Au and Pt are nearly identical,[41] this indicates some loss of the majority component during the repeated arc melting or segregation of the minority components towards the surface, (iv) there is a small shoulder at the higher binding energy side of the Pt 4f peak in Au_9Pt which is reduced upon sputtering but cannot be removed totally upon repeated sputtering, it is attributed to surface oxide in the cracks in the surface. XPS at 180 eV (more surface sensitive) and 2500 eV (more bulk sensitive) photon energy (not shown) confirm the bulk and surface origin of these peaks and finally; (v) the Pt 4f peak shape, which exhibits a significant asymmetry in Pt and Pt_9Au with the Doniach-Sunjic line shape,[24,25,44] becomes more symmetric and Au like in Au_9Pt.

Figure 2 shows the VB region of the alloys and the pure metal. As noted above, Au shows the characteristic 5d band with the d band edge at ~2 eV below the Fermi level whereas the top of the Pt 5d band is at the Fermi level. The alloy generally maintains the appearance of the host. More details will be discussed below.

Figure 3 shows the Pt and Au L_3-edge XANES of the alloy vs the pure metal. Bearing in mind that the atomic Pt L_3 edge jump is 8% larger than that of Au, the composition is close to the stoichiometry.[45] It should be noted that the Pt L_3-edge EXAFS runs underneath the Au L_3-edge XAFS which is only several hundred eV above, so that Au L_3-edge of the diluted Au alloy cannot be reliably extracted accurately and we will focus on the analysis of the Pt L_3-edge in Au_9Pt which appears to be the most interesting.

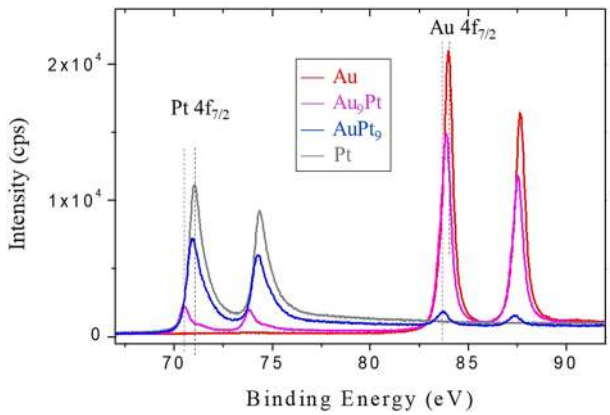

FIG. 1. Au and Pt 4f XPS spectra of Au, Au_9Pt, Pt and $AuPt_9$ (top to bottom); the dotted lines show the negative binding energy shift of both Au and Pt in the dilute alloy relative to the pure metal.

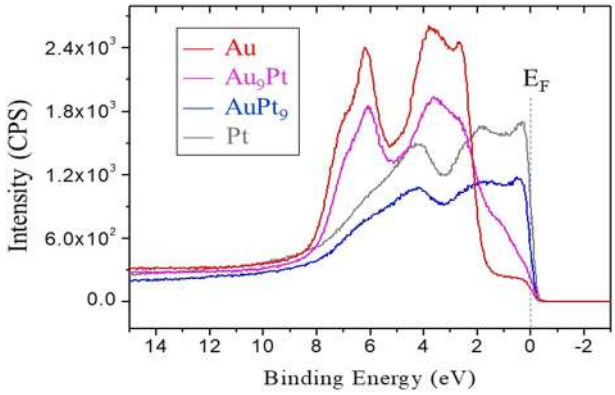

FIG. 2. Al Kα XPS VB spectra of Au, Au_9Pt, Pt and $AuPt_9$ from top to bottom; the dotted line tracks the Fermi level.

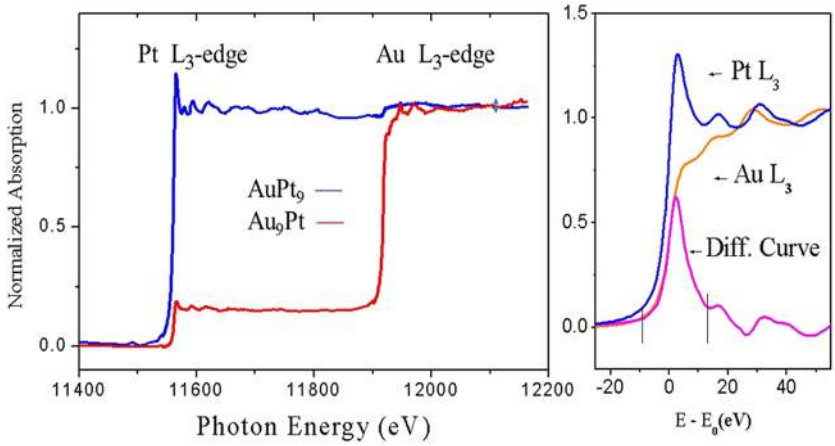

FIG. 3. Pt L_3- and Au L_3-edge XANES of Au_9Pt and $AuPt_9$ (left panel); the total edge jump is normalized to unity (absolute edge jump for the Pt L_3-edge is 8% larger than that of the Au L_3-edge). The right panel shows the L_3-edge XANES of Au and Pt metal relative to the threshold. The area under the difference curve is the experimentally determined WL intensity, which is proportional to the Pt d hole at the Fermi level.

The Au and Pt 4f binding energy shifts of the bulk alloys and relevant XPS Au 4f binding energy shift and Mössbauer IS values of PtAu alloys are summarized in Table I. It can be seen from Table I that the 4f binding energy shifts are in the same range as those reported in Au-Pt nanoparticles studies;[29] all shifts are toward the lower binding energy side relative to the pure metal and that the Mössbauer IS is slightly positive, indicating a small contact density increase in all Pt-Au bimetallic systems.[30] More detailed analysis of the data presented here will be analyzed and discussed in the next section.

IV. ANALYSIS AND DISCUSSION

A. Charge distribution at the Au/Pt site from 4f binding energy and Mossbauer IS

Let us begin the analysis of the charge redistribution at the Au site in Pt_9Au with the charge compensation model.[1] In this model, the binding energy shift between the alloy and Au, ΔBE, is related to the conduction charge gain, Δn_c, 5d charge depletion, Δn_d, a Madelung-like term due to a small net charge flow onto the Au site, δ, and volume effects if it applies and can be expressed in equation 1 below.

$$\Delta BE(alloy - Au) = -\Delta n_c F_c - \Delta n_d F_d + \delta F_{latt} + \Delta E_F + \left(\frac{dE}{dV}\right)\Delta V \quad (1)$$

where F_c and F_d are the changes in Au 4f core-electron binding energy resulting from the addition at the Au site of a single conduction or d electron, respectively.[1,2,11] The net charge flow, δ, involves the redistribution of both the conduction Δn_c, and 5d charge, Δn_d, upon alloying shown in Eq. 2.

$$\delta = \Delta n_c + \Delta n_d \tag{2}$$

A net charge flow gives rise to a Madelung-like contribution, δF_{latt}, due to the presence of this charge outside the volume of the Au atom. This term, which is a Madelung sum for an ordered compound, arises, in the case of a dilute impurity, from the placement of the transferred charge δ in the immediate neighborhood of the impurity site, after the manner of Friedel theory.[46] Eq. 1 connects the experimental binding-energy shift ΔBE (alloy-Au), which is measured relative to the Fermi level, to charge redistribution upon alloying. The ΔE_F terms, calculated relative to the crystal zero, is the Fermi level shift, taken to be the difference in work function -Δϕ (the difference in surface dipole barrier which is often small and similar in metals has been neglected in this calculation). It is often necessary to include the Δϕ term in order to bring the ΔBE, and the F_c and F_d to the same reference level in cases where the work function of the Au and host is significant different.[1–4] In this case, the work function of Au and Pt are similar, both slightly larger than 5 eV, Δϕ is neglected. A small uncertainty in this term will not affect the conclusion of the analysis (see below). The last term is for volume correction; it deals with the deviation from Vegards law[4] in volume changes affecting the BE change due to compression or expansion. In the case of Au-Pt alloys, they both have the fcc structure as in the pure metal, this term is small. Thus, equations (1) and (2) for Au-Pt alloy may be combined to the first approximation to yield

$$\Delta BE = \delta(F_{latt} - F_d) - \Delta n_c(F_c - F_d) \tag{3}$$

From Eq. 3, Δn_c at the Au site in Au-Pt alloys can be obtained from ^{119}Au Mössbauer IS using a scaling factor of Δn_c, = -0.086 IS(mms^{-1}).[14] The F values have been calculated and tested extensively to confirm the validity of the charge compensation model.[1–4,7–12] Relevant values for Au and Pt F parameters used in the analysis are given in Table II.

Using the Al Kα Au 4f data from Table I, the IS conversion, and Eqs. 2 and 3, we obtained Δn_c and δ, then the values of $\Delta n_d = \delta$ - Δn_c at the Au site in Au_9Pt. Although ^{195} Pt Mössbauer IS of Au-Pt alloy and its conversion to Δn_c are not readily available, Eq. 3 can still be used to calculate the charge redistribution at the Pt site taking into account charge conservation considerations; i.e. that charge flow onto the Au site must be balanced by the loss of charge off the Pt site; for a 50-50 alloy for example, δ(Pt) = - δ(Au) and in this work, δ(Pt) = - 9δ(Au) in Au_9Pt and δ(Pt) = - δ(Au)/9 in $AuPt_9$. The δ at the Pt site in Eq. 3 is then known and Δn_c is the unknown. The results of these analysis at both Au and Pt sites are summarized in Table III.

TABLE II. Relevant F parameters of 5d metallic elements.[a]

5d metal	F_c	F_d	F_{latt}	F_c - F_d	F_{latt} - F_d
Au (eV)	12.5	15.5	7.8	- 3.0	-7.7
Ta (eV)	11.0	13.0	7.8	- 2.0	-5.7
Pt [a](eV)	12.3	15.1	7.8	- 2.8	-7.3

[a]Interpolated values from Ta and Au F parameters in terms of 5d counts (ref. 11).

TABLE III. Conduction and d electron transfer, the dilute cases are highlighted with block numbers. Uncertainty is estimated to be ~ 10%.

Alloy		ΔBE, Au 4f (eV)	ΔBE, Pt 4f (eV)	Δn_c	δ	Δn_d
$AuPt_9$	Au site	**-0.24**		**0.067**	**0.057**	**-0.010**
$AuPt_9$	Pt site		- 0.09	-0.088	-0.006	0.082
Au_9Pt	Au site	-0.11		0.007	0.017	0.010
Au_9Pt	Pt site		**- 0.50**	**-0.577**	**-0.153**	**0.730**

It is interesting to note from Table III that charge redistribution at the Au site exhibits the following characteristics: (i) the net charge flow is small ($\delta < 0.1$ electron) and the direction of the net charge flow is in good accord with electronegativity expectation. (ii) Au gains 6s conduction charge and loses d charge in $AuPt_9$, as in the case of all Au bimetallic; the Δn_c value of 0.067 is in line with the dilute limited of 0.10 previously noted[1–4] and (iii) Au gains very small amount of charge of both s and d character in Au_9Pt. Observations (i) and (ii) are consistent with observation on other Au bimetallics with non-d and transition metals. Observation (iii) shows that the d electrons are much less involved in the rehybridization upon Au-Pt alloying (very small difference in electronegativity) and the depleted d counts are no longer sufficient to compensate the effect of the gain of the conduction electron count; as a result, the Au 4f binding energy shifts to lower binding energy. In $AuPt_9$, for example, Δn_c is ~ 7 times larger than the depleted d count, $\Delta n_{d,}$ while the F_d is only 24% larger then $F_{c.}$ Thus, the nearly constant ratio of $|\Delta n_c/\Delta n_d|$ ranging ~ 1.1 - 2.0 observed previously[4] does not hold in Au-Pt alloys.

Charge redistribution at the Pt site for Au_9Pt shows a more significant redistribution of the Pt conduction and d electrons in the direction opposite to that of the Au diluted in Pt; δ and Δn_c are in good agreement with electronegativity expectation but Δn_d is not. This is perhaps not surprising since the Pt d band is not completely filled and can easily accommodate additional d charge. The unoccupied d states just above the Fermi level in Pt provides a buffer for charge redistribution and this property makes Pt an ideal material for the design of catalyst for a desired functionality. The Δn_c and Δn_d compensation is more significant and the Pt site gains sufficient d charge to compensate the coulombic effect due to conduction charge loss at the Pt site; the net effect produces a negative binding energy shift. Since the d hole at the Pt site in nominally ~1 ($6^{s1}5d^9$, slightly varied due to s-d hybridization and band formation which can be obtained from band structure calculations),[22] the Δn_d value of 0.73 for Pt in Au_9Pt is in the right direction albeit likely an overestimate. The direction of the charge flow is unmistakably towards d charge gain at the Pt site. This d charge gain at the Pt site will fill the previously unoccupied DOS at the Pt Fermi level. This is also evident from the change of line shape from DS like in Pt metal to the more gaussian-like in $AuPt_9$, this change is associated with a reduction of unoccupied d states above the Fermi level, hence reducing the many-body effects in the 4f level excitation. The d charge gained at the Pt site in Au_9Pt is confirmed from the reduced intensity of the Pt L_3-edge WL (Fig. 3 and 6). More detailed discussions will be given in section IV–C below.

We can also apply the compensation model to interpret the negative Au 4f binding energy shift and charge redistribution in the Au-Pd bimetallic system reported in the literature.[31,32] The 4f binding energy shift and ^{197}Au Mössbauer IS of a 50-50 AuPd alloy system is used as an example, for which the ΔBE and IS have been measured as - 0.34 eV[29] and 1.06 mms^{-1},[30] respectively, the latter corresponds to $\Delta n_c = 0.09$ at the Au site. Using Eq. 3 and assuming negligible work function changes (Au, Pt and Pd all have work function slightly over 5eV depending on the specimen), we obtain $\delta = 0.08 \pm 0.01$, $\Delta n_c = 0.09 \pm 0.01$ and $\Delta n_d = -0.01 \pm 0.01$ electron count for charge redistribution at the Au site in AuPd. The errors were estimated by allowing a 20% uncertainty in the sum of the energy terms in Eq. 3 except the δ term. It is immediate apparent from this analysis that as in the case of Au_9Pt, Au in AuPd gains mostly 6s conduction charge with little 5d charge depletion ($|\Delta n_c/\Delta n_d|$ ~ 9:1) and the Au 4f binding energy shifts in the direction expected from electronegativity. Au-Pt and Au-Pd appear to be the only Au bimetallic system where Au 4f binding energy shifts are as expected from electronegativity considerations. All other Au bimetallics exhibit a positive Au 4f binding energy shift; in fact, the larger the difference in electronegativity, the more positive the Au 4f BE shift.[1–11] Thus, a trend emerges in which Au is more likely to switch on s-d charge compensation as the electronegativity difference between Au and the host increases.

B. The VB spectra and the occupied DOS below the Fermi level

The above-discussed charge redistribution can be observed in the XPS VB spectra which display the occupied DOS of both 6s and 5d character. Since the 5d electrons have a considerable higher count (cross-section) than 6s at these photon energies,[41] the d band is a dominant feature in the VB of these metals. We can see from Figure 2 that the dilute alloys exhibit patterns similar to those of pure metal, where the Au d band is broad, lies at ~2 eV below the Fermi level and shows a doublet

centred at ~ 4.6 eV below E_F with a splitting of ~ 2.6 eV, which results from the combined effect of spin-orbit and band formation and is significantly larger than the atomic spin -orbit interaction of ~ 1 eV. The 6s conduction electron is nearly free-electron like and shows as a Fermi edge at zero binding energy. The Au_9Pt VB clearly shows additional DOS just below the Fermi level not seen in pure Au and it can be attributed to the 5d character of Pt in the dilute alloy. The $AuPt_9$ VB appears to be very similar to that of the Pt metal which exhibits high occupied DOS of 5d character just below the Fermi level and a broad d band while the Au component is buried under the Pt DOS.

To better examine the contribution of Au and Pt components to the VB, we have obtained the difference curve between the VB of the alloy and the pure metal with proper scaling. Again, the similar cross section[41] of the Au and Pt 5d electrons facilitate the analysis. Fig. 4 shows the difference curve of the VB assuming that cross-section is additive. The alloy and metal VB are normalized to the most intense peak, the "apparent $d_{3/2}$ component" (BE~ 7 eV) in the d band of Au and the d band edge of Pt just below the Fermi level. The metal VB intensity is reduced to 90% prior to subtraction. This approximation is justified since the Au $5d_{3/2}$ component is least affected by alloying[47] and 90% of the alloy is the host metal. It will provide valuable information albeit semi-quantitative at best on the d-d interaction among the Au and Pt atoms in the alloy band formation. It should be noted there should still be direct Pt-Pt and Au-Au interaction at the impurity site of the dilute alloy with 10% impurity atoms, since in the fcc phase, each atom is surrounded by 12 neighboring atoms.

From Fig. 4, we see that there is a narrow and high DOS in Au_9Pt VB just below the Fermi level marked by an arrow and it must be from the Pt d band while the d character of Au host remains Au like. The difference curve in the $AuPt_9$ VB shows that while the Pt d band component remains Pt metal like, for the Au d band, despite keeping its Au metal d band like feature, the top of the d band has been pushed towards the Fermi level (marked by an arrow). This is very interesting and suggesting that the Pt d band can be easier manipulated then the Au d band. This observation is supported by DFT calculation of the DOS of $Au_{11}Pt$ and $AuPt_{11}$, as shown in the upper panels of Fig. 5, the partial densities of d states for both $Au_{11}Pt$ and $AuPt_{11}$, which clearly show that the host metal 5d band component is essentially that of the metal (not shown). In $Au_{11}Pt$, the top of the Au d band is still below the Fermi level but there is a presence of narrow and high DOS of Pt d character just below the Fermi level. In $AuPt_{11}$, while the Au d band is still Au metal like but the top of the d band has been pushed towards the Fermi level confirming the experimental observation (Fig. 4).

C. Pt $L_{3,2}$-edge and unoccupied DOS above the Fermi level in Au_9Pt

Figure 3 shows the Pt L_3-edge XANES of the Au_9Pt alloy and Pt metal. The sharp peak at the Pt L_3-edge is the well-known WL which arises from dipole electronic transition from Pt $2p_{3/2}$ to the unoccupied electronic states of Pt $5d_{5/2,3/2}$ character above the Fermi level. The area underneath

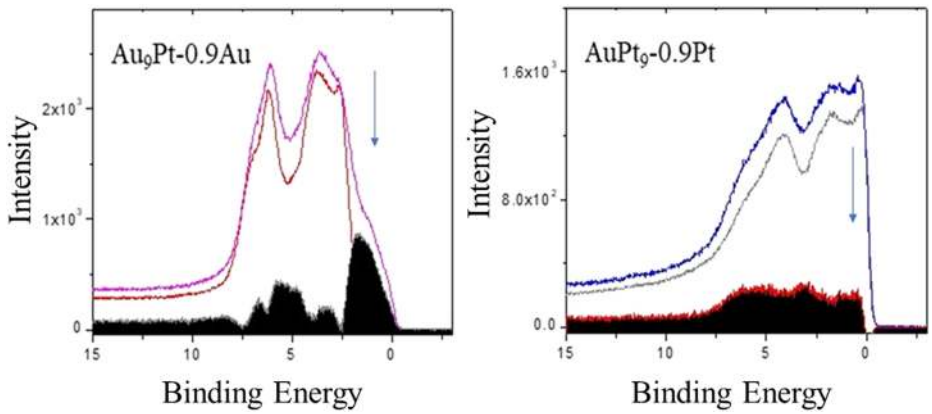

FIG. 4. Difference VB (shadowed area) between alloy and the metal (see text). Left panel: VB (Au_9Pt) - 0.9 × VB(Au); right panel: VB ($AuPt_9$) - 0.9 × VB(Pt). The difference curve represents the d band of the diluted components: Pt in Au_9Pt on the left and Au in $AuPt_9$ on the right. The arrows mark key features predicted by DFT DOS calculations.

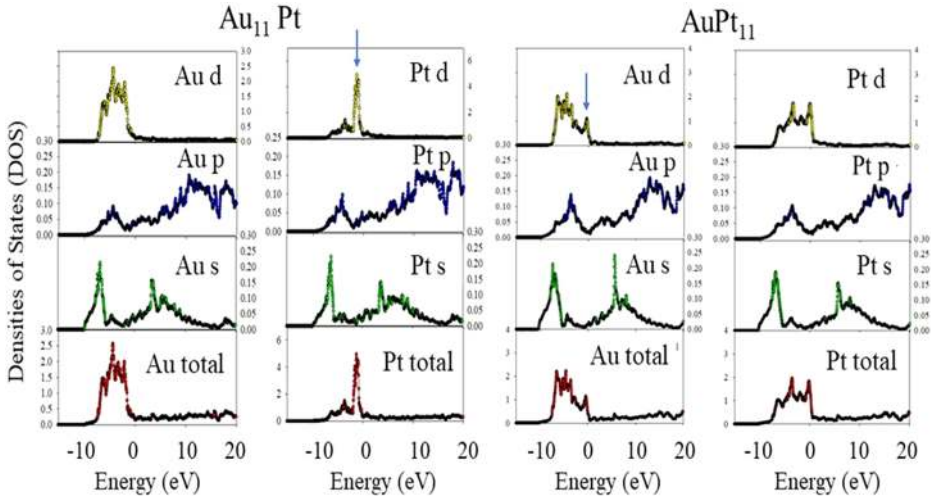

FIG. 5. DOS of $Au_{11}Pt$ and $AuPt_{11}$; Fermi level is at Energy = 0 eV. It should be noted the DOS scale for the s and p electrons has been expanded considerably, in the d DOS scale, they are less than 10% compared to d counts. The most interesting features are in the partial DOS of d character marked with arrows which are observed experimentally (Fig. 4).

the curve, often represented by the difference curve between the Pt and Au L_3-edge XANES relative to the edge jump (threshold) is shown in the left panel. Since both Au and Pt have the same fcc structure with very similar lattice constant, and the Au L_3-edge XANES exhibits no WL for the Au d band is full, this is a good approximation.[21] The Pt 5d hole can be calculated as was done by Mattheiss and Dietz,[22] leading to the following expressions relating the WL intensity to the Pt d hole counts.

$$\Delta A_3 = C_o N_o E_3 (R_d^{2p_{3/2}})^2 \left(\frac{6h_{5/2} + h_{3/2}}{15} \right) \tag{4a}$$

$$\Delta A_2 = C_o N_o E_2 (R_d^{2p_{1/2}})^2 \left(\frac{1}{3} h_{3/2} \right) \tag{4b}$$

where $C_o = 4\pi^2\alpha/3$ (α is the fine structure constant), N_0 is the density of Au atoms, $E_{2,3}$ are the absorption threshold energies, and R is the radial dipole integral. If, to the first approximation, the radial dipole moments for the two excitation processes are assumed to be equal, then the d-hole counts, $h_{5/2}$ and $h_{3/2}$ can be expressed in terms of WL intensity (area under the curve) ΔA_3 and ΔA_2 at the L_3 and L_2 edge, respectively as shown in Eq. 5.

$$h_{5/2} = \frac{1}{2C} \left(5 \frac{E_2}{E_3} \Delta A_3 - \Delta A_2 \right) \tag{5a}$$

$$h_{3/2} = \frac{3}{C} (\Delta A_2) \tag{5b}$$

where $C = C_o N_o E_2 \left(R_d^{2p} \right)^2$. It is well known that in Pt and Au, the 5d spin orbit interaction is large and $5d_{5/2}$ and $5d_{3/2}$ characters are separated; for example, in Pt the unoccupied 5d states are primarily of $d_{5/2}$ character.[20,21] Thus, to fully evaluate the d hole count using Eq. 5, we also need to obtain the WL intensity from the Pt L_2-edge XANES. As noted above, the Au L_3-edge data (E_o = 11919 eV) suffer from uncertainty arising from the presence of preceding Pt L_3-edge EXAFS (E_o = 11564 eV); fortunately for the Pt L_2-edge (E_o =13273 eV), the preceding Au L_3-edge is far away and will not contribute significantly to the Pt L_2-edge data. The Pt $L_{3,2}$-edge XANES are shown in Figure 6, which show little change at the Pt L_2-edge WL but the post edge oscillations change noticeably. It is interesting to note that this behaviour has also been observed in Pt-Au nanowires.[28]

Let us first concentrate on the WL region. It is immediately apparent that there exhibit a significant reduction of WL intensity at the Pt L_3-edge of Au_9Pt, indicating that Pt gains 5d charge at the Pt site in Au_9Pt. This observation is in excellent agreement with the analysis of the charge compensation

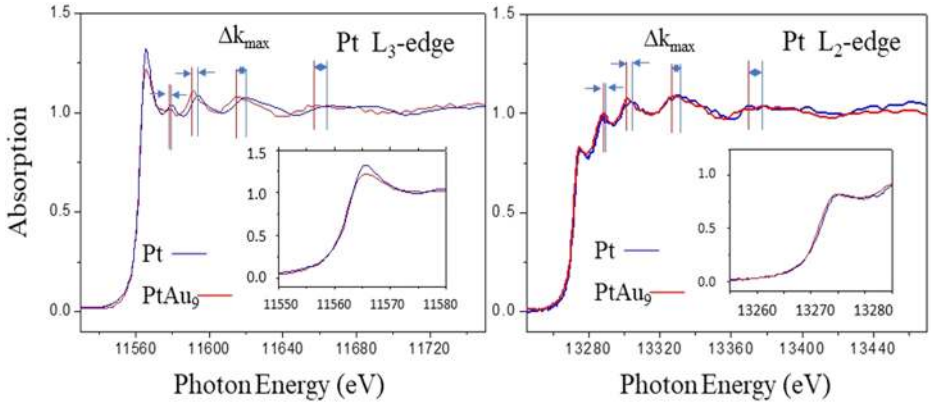

FIG. 6. Pt $L_{3,2}$-edge XANES of $AuPt_9$ compared with Pt metal. The inset shows the WL region; the vertical bars mark the oscillation maxima of the EXAFS of the alloy and the metal in energy and momentum (k) space; the progressively increase in separation between the alloy and the metal, Δk_{max} is marked with horizontal double arrows.

model which shows that Pt gains 5d charge, and with the VB and DFT results, which show DOS of significant Pt 5d character just below the Fermi level.

It is also interesting to note that despite a significant reduction in the alloy WL at the Pt L_3-edge, the Pt L_2-edge WL region exhibits no WL and no change upon alloying confirming that in the alloy, the $5d_{3/2}$ is full as in the pure metal and the active 5d character is $5d_{5/2}$. Thus, to a good approximation, the Pt 5d hole change in Au_9Pt can be expressed as,

$$h_{5/2} = \frac{5E_2}{2CE_3}\Delta A_3 \tag{6}$$

Equation (6) in principle can be used to evaluate the $5d_{5/2}$. hole count at the Fermi level. Alternatively, one can extract empirically from a recent Pt $L_{3,2}$-WL study of Pt single atom to small clusters[27] to arrive at the following linear relationship using a linear fit of four sets of ΔA_3, $h_{5/2}$ values (5.61, 0.511; 6.18, 0.558; 7.19, 0.646; 7.73, 0.703).

$$h_{5/2} = 0.0899\Delta A_3 + 0.00422 \tag{7}$$

where the slope (±0.0029) and the intercept (±0.019) with $R^2 = 0.99696$ for the goodness of the fit were obtained from the linear fit of the ΔA_3 and $h_{5/2}$ hole values, showing that it is a very good fit. Analysis of the Pt L_3-edge WL of Au_9Pt shows that the area under the WL $\Delta A_3 = 4.62$ as illustrated in Figure 2 (subtracting a Au L_3-edge XANES) is 88% of that of the Pt or 12% reduction. Using Eq. 6, one arrives at a $h_{5/2}$ value of 0.42 for Au_9Pt or $\Delta n_{d(5/2)}$ of -0.1. This result not only confirms qualitatively the direction of 5d charge depletion at the Pt site deduced from the compensation model analysis but also shows that the d charge is primarily of $5d_{5/2}$ character.

There are additional features in Figure 6 that are worth noting. These are the progressively increasing separation of the EXAFS oscillation maxima, Δk_{max} which are observed in both Pt L_3-and L_2-edges. The Pt site in Au_9Pt exhibits EXAFS oscillations with maximum closer to the threshold. Generally, as a well-known behavior of EXAFS, the closer the oscillation maxima, the longer the bond. Since Au and Pt have similar k dependence in both backscattering amplitude and phase, this behavior observed in Au_9Pt then shows, at least qualitatively, that locally, the Pt-nearest neighbor (mostly Au, including Pt) interatomic distance is longer than those in pure Pt metal. This observation is consistent with the fact that Au has a slightly larger lattice constant (4.08 Å) than Pt (3.92 Å); this local expansion facilitates the gain of the more diffused d charge in Pt, in addition to a small electronegativity difference.

V. CONCLUSION

From XPS and XAS measurements on Au-Pt alloys, $AuPt_9$ and Au_9Pt, we observe a negative 4f binding energy shift of the Au and Pt in the alloy relative to the pure metal. This observation

is in contrast to a large number of previous observations in which the Au 4f binding energy in Au bimetallic shift to higher binding. Analysis of these data together with Mössbauer results using a charge compensation model show that Au gain a very small net charge of main 6s conduction character in $AuPt_9$ with very little d charge depletion. As for Pt in Au_9Pt, Pt loses s charge and gains d charge. Both VB spectra and DFT calculations support these results. The Pt d charge gain is of primarily $5d_{5/2}$ character as revealed from the analysis of the Pt $L_{3,2}$-edge WL. Similar analysis performed on a previously reported Au-Pd system shows that its behaviour is similar to that of the Au-Pt system, both have small electronegativity difference from Au. What emerges on the analysis of the Au-Pt and Au-Pd data together with all Au bimetallic system previously studied is that we have considered all possible scenarios of s-d charge compensation for all possible cases of Au 4f binding energy shifts in bimetallic alloys. Thus, Au bimetallic systems of any combination (intuitively or counter intuitively to electronegativity consideration) can now be readily analyzed taking into account the mechanism described here; that is that Au bimetallic systems can be tracked by s-d hybridization and charge compensation which is triggered primarily by the difference in the electronegativity between Au and its counter part in a bimetallic system: at small electronegativity difference, charge transfer is mainly 6s conduction character, as the counter component becomes more electropositive, d-charge depletion will take place to offset the 6s conduction flow to maintain electroneutrality locally. These results will have interesting implications for the understanding of bimetallic alloys and nanostructures containing Au and Pt as well as noble metal bimetallic systems and their performance in given functionalities.

ACKNOWLEDGMENTS

The authors acknowledge Jim Garret of the Brockhouse Institute of Materials Research for the preparation of the bulk alloys. Synchrotron experiments were conducted at the Canadian Light Source supported by CFI, NSERC, NRC, CIHR and the University of Saskatchewan, and at the Advanced Photon Source, Argonne National Laboratory, supported by the US Department of Energy. We thank Mark Beisinger of Surface Science Western for making the lab XPS measurements. Research at the University of Western Ontario is supported by NSERC Discovery, NSERC Strategic Partnership, CFI and Canada Research Chair (TKS).

[1] R. E. Watson, J. Hudis, and M. L. Perlman, Phys. Rev. B **4**, 4139 (1971).
[2] R. M. Friedman, J. Hudis, M. L. Perlman, and R. E. Watson, Phys. Rev. B **8**, 2433 (1973).
[3] T. S. Chou, M. L. Perlman, and R. E. Watson, Phys. Rev. B **14**, 3248 (1976).
[4] T. K. Sham, M. L. Perlman, and R. E. Watson, Phys. Rev. B **19**, 539 (1979).
[5] T. K. Sham, R. E. Watson, and M. L. Perlman, Phys. Rev. B **20**, 3552 (1979).
[6] D. T. Jiang, T. K. Sham, P. R. Norton, and S. M. Heald, Phys. Rev. B **49**, 3709 (1994).
[7] T. K. Sham, Y. M. Yiu, M. Kuhn, and K. H. Tan, Phys. Rev. B **41**, 11881 (1990); Erratum **42**, 9194 (1990).
[8] C. C. Tyson, A. Bzowski, P. Kristof, M. Kuhn, R. Sammynaiken, and T. K. Sham, Phys. Rev. B **45**, 8924 (1992).
[9] M. Kuhn and T. K. Sham, Phys. Rev. B **49**, 1647 (1994).
[10] A. Bzowski and T. K. Sham, J Vac. Sci. Tech. A **11**, 2153 (1993).
[11] M. Kuhn, R. Sammynaiken, and T. K. Sham, Physica B **252**, 114 (1998).
[12] R. E. Watson and L. H. Bennett, Phys. Rev. B **15**, 502 (1977).
[13] D. A. Shirley, Rev. Mod. Phys. **36**, 339 (1964).
[14] T. K. Sham, R. E. Watson, and M. L. Perlman, *Mössbauer Spectroscopy and Its Chemical Applications, Advances in Chemistry* (American Chemical Society, 1981), Vol. 194, 39–60.
[15] J. O. Thomson, F. E. Obenshain, and P. G. Huray, Phys. Rev. B **11** (1975).
[16] A. Bzowski, Y. M. Yiu, and T. K. Sham, Phys. Rev. B **51**, 9515 (1995).
[17] M. Kuhn, A. Bzowski, and T. K. Sham, Hyperfine Interactions **94**, 2267–2272 (1994).
[18] R. E. Watson, J. W. Davenport, and M. Weinert, Phys. Rev. B **35**, 508 (1987).
[19] M. Weinert and R. E. Watson, Phys. Rev. B **51**, 17168 (1955).
[20] N. Mott, Proc. Royal Society.
[21] M. Brown, R. E. Peierls, and E. A. Stern, Phys. Rev. B **15**, 738 (1977).
[22] L. F. Mattheiss and R. E. Dietz, Phys. Rev. B **22**, 1663 (1980).
[23] A. N. Mansour, J. W. Cook, and D. E. Sayers, J. Phys. Chem. **88**, 2330–2334 (1984).
[24] S. Doniach and M. Sunjic, J. Phys. **4C31**, 285 (1970).
[25] G. Wertheim, J. Electron Spectrosc. **6**, 239 (1975).
[26] S. Sun, G. Zhang, X. Meng, M. Norouzi Banis, D. Geng, R. Li, X.-L. Sun, N. Gauquelin, Botton, N. Chen, J. Zhou, S. Yang, W. Chen, T.-K. Sham, and X. Sun, Sci. Rep. **3**, 1775 (2013).
[27] N. Cheng., S. Stambula, D. Wang, M. N. Banis, J. Liu, A. Riese, B. Xiao, R. Li, T.-K. Sham, L.-M. Liu, G. A. Botton, and X. Sun, Nature Communications **7**, 13638 (2016).
[28] T. K. Sham, M. J. Ward, M. W. Murphy, L. J. Liu, and W. Q. Han, J. Phys.: Conf. Ser. **430**, 012018 (2013).

[29] W. Ye, H. Kou, Q. Liu, J. Yan, F. Zhou, and C. Wang, International Journal of Hydrogen Energy **37**, 4088 (2012).
[30] M. Nakanishi, H. Takatani, Y. Kobayashi, F. Hori, R. Taniguchi, A. Iwase, and R. Oshima, Appl. Surf. Sci. **241**, 209 (2005).
[31] P. A. P. Nascente, S. G. C. de Castro, R. Landers, and G. G. Kleiman, Phys. Rev. B **43**, 4659 (1991).
[32] H. Takatani, H. Kago, M. Nakanishi, Y. Kobayashi, F. Hori, and Oshima, Rev. Adv. Mater. Sci. **5**, 232 (2003).
[33] P. M. Hansen, *Constitution of Binary Alloys*, 2nd ed. (McGraw-Hill, New York, 1958).
[34] Y. F. Hu, L. Zuin, R. Reininger, and T. K. Sham, AIP Conference Proceedings **879**, 535 (2007).
[35] Q. Xiao, X. Cui, Y. Shi, Y. Hu, T.-K. Sham, H. Piao, and J. McMahon, Can. J. Chem. **93**, 113 (2015).
[36] W. Kohn and L. J. Sham, Phys. Rev. **140**, A1133 (1965).
[37] J. P. Perdew and Y. Wang, Phys. Rev. B **45**, 13244 (1992).
[38] P. Blaha, K. Schwarz, P. Sorantin, and S. B. Trickey, Computer Phys. Comm. **59**, 399 (1990).
[39] Y. M. Yiu, Chapter 2 of Part I in "*Applications of Chalcogenides: S, Se, and Te*", edited by G. K. Ahluwalia, Springer International Publishing Switzerland (2017).
[40] J. P. Perdew, S. Burke, and M. Ernzerhof, Phys. Rev. Let. **77**, 3865 (1996).
[41] J. J. Yeh and I. Lindau, Atomic Data and Nuclear Data Tables **32**, l (1985).
[42] X-ray calculator- http://henke.lbl.gov/optical_constants/.
[43] P. H. Citrin and G. K. Wertheim, Phys. Rev. B **27**, 3176 (1983).
[44] S. J. Naftel, A. Bzowski, and T. K. Sham, J. Alloys and Compounds **283**, 5 (1999).
[45] W. H. McMaster, N. K. Del Grande, J. H. Mallett, and J. H. Hubbell, "Compilation of x-ray cross sections," Lawrence Livermore National Laboratory Report UCRL-50174.
[46] J. Friedel, Philos. Mag. **43**, 153 (1952).
[47] A. Bzowski, M. Kuhn, T. K. Sham, J. A. Rodriguez, and J. Hrbek, Phys. Rev. B **59**, 13379 (1999).